Monte Carlo Statistical Mechanical Simulations of the Competition of Intermolecular Electrostatic and Poling-Field Interactions in Defining Macroscopic Electro-Optic Activity for Organic Chromophore/Polymer Materials†

B. H. Robinson and L. R. Dalton*

Department of Chemistry, University of Washington, Seattle, Washington 98195-1700

Received: November 4, 1999; In Final Form: February 15, 2000

Monte Carlo statistical mechanical computer simulations of the electric-field poling of second-order nonlinear optical chromophores, characterized by large dipole moments, polarizabilities, and hyperpolarizabilities, are presented. Such theoretical analysis is critical to defining the structure/function relationships that permit maximization of electro-optic activity for π-electron chromophore-containing polymeric materials. Polymeric electro-optic materials may, in turn, be important for high-bandwidth telecommunications, new forms of radar, and high-speed data processing. The experimentally observed maxima in plots of electro-optic activity versus chromophore number density (loading) in polymer matrices are theoretically reproduced, as are the shifts of the maxima to lower loading with increasing chromophore dipole moment. Modification of the chromophore shape to realize the maximum achievable electro-optic activity for a given π-electron structure is discussed, as is the role of polymer electrical permittivity. Monte Carlo results are compared with the results of equilibrium statistical mechanical calculations based on the approximation of Piekara. The theoretical results presented here have led to the production of polymeric electro-optic materials that permit devices with drive voltage requirements of less than 1 V to be fabricated. Polymeric modulators now significantly exceed the performance capabilities (in terms of bandwidth and drive voltage) of electro-optic modulators based on inorganic materials.

Introduction

Since the 1930s, considerable theoretical attention has been focused on understanding the role of intermolecular electrostatic interactions in defining physical properties of matter and, particularly, of condensed phase matter.[1] Two different types of properties are normally the subject of such considerations. More commonly, scientists have focused on "aggregation" or "association" effects involving condensation of particles (atoms, ions, and molecules) onto surfaces, phase changes of the physical state of matter, or phase-separation phenomena. Less frequently, theorists have considered "orientational" effects associated with the competition between an applied field and intermolecular electrostatic interactions in defining an orientation-dependent variable such as the dipole moment. Treating the interaction of a large ensemble of particles (atoms, molecules, and ions) is, in general, a formidable undertaking, so it is not surprising that these two different problems have evoked quite different treatments (and approximations). For the consideration of field-independent aggregation or association effects, orientation-independent potential functions are typically utilized. Use of such isotropic potential functions is not appropriate when relevant physical properties depend on the presence of an externally applied field (such as an electric field, used when measuring the dipole moment of a material, or a magnetic field, used when measuring multi-quantum excitations in a dipolar spin system). For modeling such physical properties, theorists are faced with the additional complexity of how a multiplicity of orientational variables (relating particles to the applied field and to each other) should be treated. Because of the additional computational complexity and the reduced frequency with which field-dependent phenomena are encountered in the physical world, it is not surprising that the theoretical "maturity" or "sophistication" of treating field-dependent (or orientation-dependent) phenomena is less than that of treating field-independent phenomena. Nevertheless, an understanding of a number of important physical phenomena, ranging from photorefractivity of organic materials to thresholdless antiferroelectric liquid crystallinity, relies on an appropriate consideration of the orientational dependence of intermolecular electrostatic interactions and molecule-applied field interactions.[2] Indeed, it has recently been observed that addition of high-dipole moment molecules to liquid crystalline materials can lower switching voltages; the addition of such molecules to organic light-emitting diode (OLED) materials can be used to tune the color of emission across the visible spectrum. Such technologically important observations provide a new incentive for understanding orientational effects dependent on both externally applied fields and intermolecular electrostatic interactions. Here, we attempt to understand one such technologically important application: the dependence of the macroscopic electro-optic activity on the density or loading into polymer matrices of molecules that have large hyperpolarizabilities and dipole moments. This is an example of competition between an externally applied electric field and the internal intermolecular dipolar interactions to create an acentric order of dipoles within the material.

Why is this a technologically important theoretical undertaking? For more than a decade, organic electro-optic materials have held the promise of having a dramatic impact on a number of technologies, including, for example, satellite and fiber telecommunications, new forms of radar, optical gyroscopes for

† Part of the special issue "Electronic and Nonlinear Optical Materials: Theory and Modeling".

* Corresponding author. E-mail: dalton@chem.washington.edu.

10.1021/jp993873s CCC: $19.00
Published on Web 04/19/2000

guidance systems, radio frequency distribution, ultrafast computation, and data processing (e.g., analog-to-digital conversion). Organic electro-optic materials have been touted as having unprecedented bandwidths, being easy to integrate with both semiconductor VLSI chips and silica optical transmission fibers, and being compatible with devices with sub-1-V drive voltage requirements.[3] Because of modest and frequency-independent dielectric constants and indices of refraction (both determined by the π-electron nature of organic electro-optic chromophores), the ultrahigh-bandwidth capabilities of organic electro-optic materials have been quite easily realized. Devices exhibiting operational (flat response) bandwidths of greater than 100 GHz have been demonstrated, and pulsed techniques have been used to establish that fundamental material bandwidths exceed 350 GHz (for a 1-cm device).[3,4] Efficient integration with VLSI semiconductor electronics and silica fibers (also with semiconductor lasers) has permitted "opto-chip" packages to be fabricated.[5] Indeed, sophisticated three-dimensional passive/active circuits[3,5] and novel devices[3−6] are now routinely fabricated. Phased-array radar systems[7] have been fabricated, and 100 Gbit/s analog-to-digital conversion[8] has been achieved. The thermal and photochemical stability of polymeric electro-optic modulators can be excellent for modulators operating at telecommunication wavelengths (1.3 and 1.55 μm). Modulators have been operated by companies such as TACAN Corporation (Carlsbad, CA) for periods of more than 4 years with no degradation in performance.[3,9] With appropriate lattice-hardening chemistry, polymeric electro-optic modulators can be heated to 200 °C before electro-optic activity is observed to decrease because of randomization of molecular orientation.[3,9−11] With appropriate attention to materials processing during device fabrication, the insertion loss of polymeric electro-optic modulators can be comparable to that of lithium niobate and greatly superior to that of gallium arsenide electro-absorptive modulators.[3] Cross talk between polymeric electro-optic modulators in high-density, multi-modulator packages is immeasurably low ($<$50 dB).[6] Bias voltage stability, radiation hardness, and other auxiliary properties of polymeric electro-optic modulators are excellent; they are clearly suitable for satellite (space) applications and other applications in moderately harsh environments.[3,10]

The most severe, and unanticipated, problem encountered in fabricating polymeric electro-optic modulators is that of translating the large hyperpolarizability of organic chromophores into large macroscopic electro-optic activity in chromophore-containing polymeric materials. If intermolecular electrostatic interactions do not come into play, macroscopic optical nonlinearity should scale as $\mu\beta$/MW, where μ is the chromophore dipole moment, β is the molecular first hyperpolarizability, and MW is the chromophore molecular weight (mass). During the preceding decade, quantum mechanical calculations helped guide greater than 250-fold improvement in $\mu\beta$ values of chromophores being considered for electro-optic applications.[3,11] However, until recently, electro-optic coefficients for polymeric electro-optic materials have remained relatively static and have failed to surpass that of lithium niobate (30−35 pm/V). This has posed a severe problem for the application of polymeric materials, as drive voltages (V_π, the voltage required for a phase shift of π) for devices fabricated from polymeric materials have remained high (6−20 V). Such high drive voltages are incompatible with semiconductor electronics. The use of high drive voltage polymeric electro-optic modulators requires the utilization of low noise amplifiers (LNAs) to boost the voltage to an appropriate level. The bandwidth limitations of LNAs eliminate the high-bandwidth advantage of polymeric electro-optic modulators. Table 1 summarizes the bandwidth and drive voltage requirements for several well-known applications of electro-optic modulators. Clearly, electro-optic materials capable of yielding sub-1-V modulators are required for wide commercial applications of electro-optic modulator technology.

TABLE 1: Drive Voltage and Bandwidth Requirements for Several Anticipated High-Volume Applications of Electro-Optic Modulators

application	bandwidth requirement	drive voltage requirement
cable TV & datacom	lower GHz	5−10 V
telecom	higher GHz	2−3 V
RF photonics	higher GHz	0.1−1.0 V

Fortunately, just as quantum mechanical calculations have guided the development of improved electro-optic chromophores, statistical mechanical considerations of intermolecular electrostatic interactions have provided a breakthrough in translating large microscopic hyperpolarizability to large macroscopic electro-optic activity. Recently, researchers at TACAN Corporation have demonstrated (with chromophore/polymer materials obtained from our laboratory) polymeric electro-optic modulators characterized by drive voltages of 0.8 V, material optical loss of 1 dB/cm, and thermal stability to 120 °C.[12] The TACAN results have recently been equaled by researchers[13] at Lockheed-Martin (Palo Alto, CA) using a different, but similar, chromophore/polymer material (also from our laboratory). Moreover, the Lockheed-Martin device has shown no degradation in performance over a period of 3 months. Device bandwidths of 100 GHz have been straightforwardly realized, and now, 100-GHz modulators are commercially available from Pacific Wave Industries (Los Angeles, CA). These modulators and modulator packages (e.g., 12 modulators per wafer) meet or exceed the performance specifications of the new Lucent 35-GHz-bandwidth lithium niobate modulators (6-V drive voltage requirement, thermal stability specified to 85 °C). In this article, we review the theory that has permitted the impressive improvements in polymeric electro-optic materials during the past year and that suggests that 0.1-V polymeric electro-optic modulators are an attainable goal.

The fundamental nature of the problem of translating microscopic molecular first hyperpolarizability, β, into large macroscopic electro-optic activity, r_{33}, is illustrated in Figures 1 and 2 for the CLD and FTC chromophore/polymer systems. A CLD-type chromophore [in poly(methyl methacrylate)] was used by TACAN to construct the first sub-1-V electro-optic modulator. An FTC chromophore [in APC, polybisphenol A carbonate-*co*-4,4′-(3,3,5-trimethylcyclohexylidene)diphenol] was used by Lockheed-Martin to fabricate their 1-V electro-optic modulators. As shown for the CLD/PMMA and FTC/PMMA chromophore/polymer matrix systems of Figures 1 and 2 (and observed for every chromophore-containing material with chromophores of dipole moments greater than 7 D; e.g., see Figure 3 and Table 2), a maximum is observed in the plot of the macroscopic electro-optic coefficient, r_{33}, versus chromophore loading (or number density, N). Moreover, the position of this maximum is observed to depend on such electrostatic parameters as the chromophore dipole moment μ. The position of the maximum electro-optic coefficient shifts to lower loading with increasing chromophore dipole moment (see Figure 3). The position of the maximum also depends on chromophore shape, even for chromophores in which the π-electron framework is the same (see Figures 1 and 2). Removal of the isophorone group protecting the polyene bridge of CLD results in a lowering of

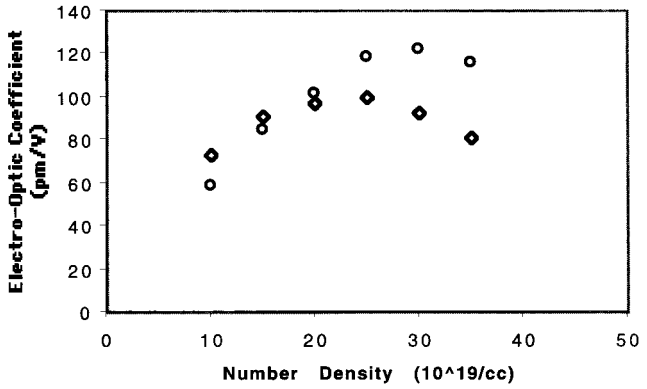

Figure 1. Variation of material electro-optic activity (r_{33}) with chromophore number density (N) for composite materials consisting of the CLD chromophores in poly(methyl methacrylate). Circles are for the variant (referred to as CLD) with an isophorone group protecting the polyene bridge structure (see Table 2). Diamonds are for the variant with no isophorone protection, i.e., a simple polyene bridge. Note that the maximum achievable electro-optic activity for the simple polyene bridge structure is smaller and is shifted to lower loading than that for the isophorone variant. This clearly indicates the shape dependence discussed in the text. Data are shown for a measurement wavelength of 1.06 μm, and measurements were carried out using a modified attenuated total reflection (ATR) technique.[3]

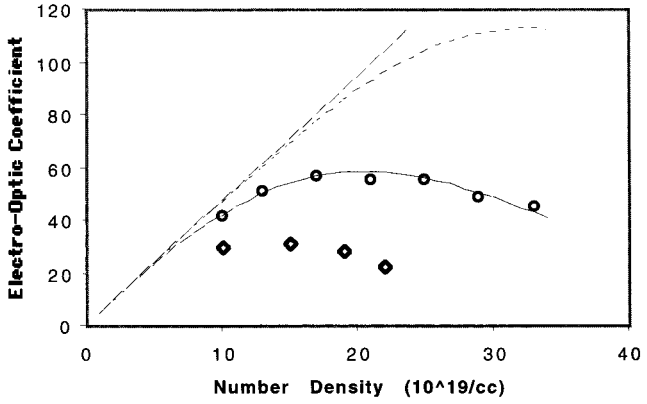

Figure 2. Variation of material electro-optic activity (r_{33}) with chromophore number density (N) for composite materials consisting of the FTC chromophores in poly(methyl methacrylate). Circles are for the variant (called FTC) with butyl groups attached to the thiophene of the bridge (see Table 2). Diamonds are for the variant (referred to as FTC-2H) in which the Bu groups have been replaced by H groups. Note that the maximum achievable electro-optic activity for the simple unprotected bridge structure is smaller and is shifted to lower loading than that for the bridge with butyl derivatization. This clearly indicates the shape dependence discussed in the text. Also shown are three equilibrium statistical mechanical theoretical results. The straight line represented by long dashes corresponds to the noninteracting chromophore model.[3] The line consisting of short dashes corresponds to full treatment of intermolecular electrostatic interactions within the framework of treating chromophores as spheres (see text).[3,9] The solid line corresponds to full consideration of intermolecular interactions within the framework of treating chromophores as hard (noninterpenetrating) ellipsoids.[3,9] Experimental data are shown for a measurement wavelength of 1.06 μm, and measurements were carried out using a modified attenuated total reflection (ATR) technique.[3]

the maximum achievable electro-optic activity, as is evident from a consideration of Figure 1 and as noted recently by Gunter and co-workers.[14]

The above observations argue for the role of chromophore−chromophore intermolecular electrostatic interactions in defining achievable macroscopic electro-optic properties. Indeed, we have carefully ruled out other concentration-dependent phenomena such as ionic conductivity.[3]

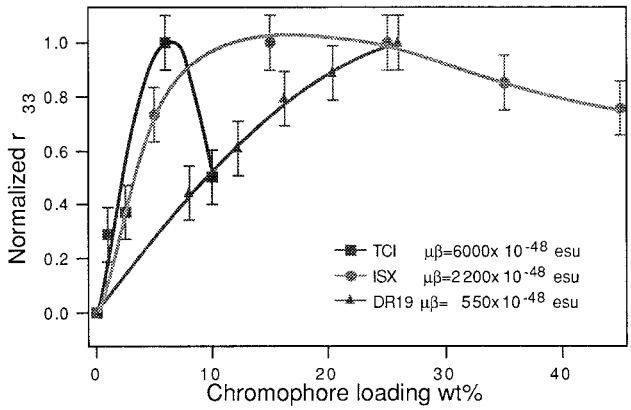

Figure 3. Variation of normalized electro-optic activity ($r_{33}/r_{33,MAX}$) as a function of chromophore loading (wt/wt %) for three chromophores. DR stands for Disperse Red, which is a chromophore consisting of an aniline donor connected by an azo bridge to a nitrobenzene acceptor.[3] Data for DR are represented by triangles. The dipole moment of this material is 7.0−7.5 D. The DR chromophore structure undergoes rapid trans−cis−trans interconversion under poling conditions, so that its shape approximates that of a sphere. The structure of the ISX chromophore[3] is given in Table 2, along with its dipole moment (theory and experiment are in reasonable agreement). Modifying ISX to make it more spherical (see JH chromophore of Table 2) leads to 4-fold improvement in the maximum achievable electro-optic activity, and the maximum in the curve is shifted to significantly higher loading. Removal of the polyene-protecting isophorone group of the JH chromophore leads to a reduction in the maximum achievable electro-optic activity, in quantitative agreement with theory.[3] The TCI chromophore[3] is intermediate between the ISX and FTC series in terms of electrostatic interactions. Experimental data are shown for a measurement wavelength of 1.06 μm, and measurements were carried out using a modified attenuated total reflection (ATR) technique.[3]

TABLE 2: Structures and Calculated Dipole Moments

	Chromophore	Dipole Moment (μ)* R=H
ISX	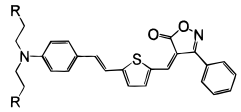	8.6021
JH	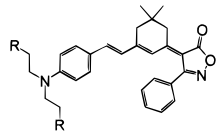	10.2698
FTC	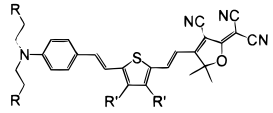	12.1898
CLD	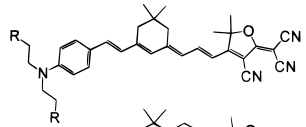	13.4668
GLD	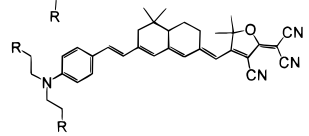	13.8811

*Dipole moment values (in D) were calculated using Spartan (Wavefunction, Inc.); theoretical values are in reasonable agreement with experimental values.

From a theoretical standpoint, the problem of explaining experimental observations can be envisioned as an issue of computing the orientational distribution (or the order parameter, $<\cos^3\theta>$, describing that distribution) for an ensemble of

interacting chromophores in the presence of an applied electric (poling) field and existing in a medium of uniform dielectric constant. For dipolar chromophores in an electric poling field, the electro-optic coefficient in the direction of the applied field (r_{33}) is related to the molecular first hyperpolarizability (β) by[15]

$$r_{33} = |2NF(\omega)\beta<\cos^3\theta>/n^4| \quad (1)$$

where N is the chromophore number density (molecules/cm^3) in the polymer host, n is the index of refraction of the chromophore-containing polymeric material, and $F(\omega)$ is the product of local-field (Debye−Onsager) factors.[15] The acentric order parameter, $<\cos^3\theta>$, relevant to calculation of electro-optic activity (r_{33}) can be computed from a consideration of all forces (enthalpic contributions) affecting the Gibbs distribution function (or statistical mechanical partition function) according to the general prescription for calculating an order parameter of order n.[16]

$$<\cos^n\theta> = \int \cos^n\theta\, G(\Omega,E_p)\, d\Omega / \int G(\Omega,E_p)\, d\Omega \quad (2)$$

where $G(\Omega,E_p)$ is the Gibbs distribution function (partition coefficient) given by

$$G(\Omega,E_p) = \exp[-U(\Omega,E_p)/kT)] \quad (3)$$

and where E_p is the electric poling field, k is the Boltzmann constant, and T is the Kelvin (poling) temperature. U is the total electrostatic potential energy, i.e., the sum of the chromophore dipole moment−electric poling field interaction and the chromophore−chromophore intermolecular electrostatic interactions. If intermolecular electrostatic interactions are neglected or if N is sufficiently small, $U = -\mu F \cos\theta$ [where F is the poling field felt by the chromophores, $F = f(0)\, E_p$, and θ is the angle between the poling field and the chromophore principal axis]. The general expression for order parameters becomes

$$<\cos^n\theta> = L_n(f) \quad (4)$$

where L_n is the nth-order Langevin function[1] and $f = \mu F/kT$. When f is small, $<\cos^1\theta> = -f/3$ and $<\cos^3\theta> = -f/5$. When $f = 0$, $<\cos^n\theta> = \delta_{n,\text{even}}/(n+1)$. Neglect of intermolecular electrostatic interactions results in the following expression in the low field limit ($f \ll 1$) for the electro-optic coefficient

$$r_{33} = 2\mu\beta N f(0)\, E_p\, f(\omega)/5kTn^4 \text{ and } N = w\rho N_A/\text{MW} \quad (5)$$

where w is the weight fraction of chromophore in the polymer lattice, MW is the molecular weight (mass) of the chromophore, ρ is the material density, and N_A is Avogadro's number. Clearly, when the intermolecular electrostatic interactions are neglected, the electro-optic coefficient (r_{33}) should increase linearly with weight fraction (w) and with dipole moment (μ).

In this article, our focus is the explicit treatment of intermolecular electrostatic interactions and their competition with molecular dipole−poling field interactions to determine $<\cos^3\theta>$. There are two logical statistical mechanics approaches to this problem. The first is the general prescription of equilibrium statistical mechanics given by eq 2. The second is to follow a Monte Carlo or molecular dynamics approach. The latter approach has the advantages of permitting all order parameters to be obtained in a single calculation and of providing more insight into the details of the distribution of chromophores. For example, nonequilibrium phenomena such as phase separation can be observed more directly with a Monte Carlo approach. There is an advantage in pursuing both approaches to the problem in that the results of the two methods can be compared, thereby providing insight into the validity of approximations employed. In the following sections of this article, we introduce and compare the two approaches to understanding electro-optic activity arising from interacting chromophores existing in the presence of a poling field. To facilitate comparison of the methods and to illustrate that even the simplest treatments qualitatively reproduce the essential features of experimental data, we initially restrict our consideration to spherical chromophores and neglect medium effects. At the end of our discussion, we briefly consider shape effects. We also initially limit our consideration to dipole−dipole interactions, neglecting induced dipole and dispersion interactions. The effects of the chromophore shape, the dielectric nature of the host medium (polymer), and the full electrostatic chromophore interactions have been treated elsewhere using an equilibrium statistical mechanics approach.[17] Also in this article, we present a quantitative simulation of data for a CLD/PMMA-type material. The agreement between theory and experiment demonstrates that shape effects can be appropriately taken into account and that quantitative simulation of experimental data can be achieved without adjustable parameters.

Before we review our computational approaches, it is appropriate to review the theoretical efforts of others aimed at understanding poling-induced electro-optic activity. Katz and co-workers[18] have applied an equilibrium thermodynamical treatment to the problem of nonlinear behavior of electro-optic activity with chromophore loading. They assume a two-state equilibrium consisting of free and aggregated chromophores. For the system studied in their work, they conclude that such a model does not represent an improvement in the simulation of experimental data. We have applied the model of Katz and co-workers to a number of high-$\mu\beta$ chromophore systems without success. The theoretical results presented in the following sections of this article explain why the model of Katz and co-workers does not work for most systems but suggest that there may be cases where it can be successfully applied.

Marks, Ratner, and co-workers[19] have performed elegant quantum mechanical analyses of the problem of dimer formation involving zwitterionic chromophores. This class of materials represents an extreme of the situation considered here. As the data presented in the following sections indicate, most high-$\mu\beta$ chromophores do not exist experimentally in a regime where aggregation is favored. Our theoretical results can be viewed as providing the bridge between the independent-particle regime and the strong-pairing (aggregation) regime studied by Mark, Ratner, and co-workers.

Kim and Hayden[20] have recently published the results of fully atomistic modeling of an electric-field-poled, guest−host nonlinear optical polymer system. Their work provides considerable insight into the interaction of chromophores with various segments of a polymer host. Results are given for temperatures above and below the glass transition temperature of the material, and the effects of side-chain and main-chain polymer segments on chromophore order are found to differ for these two regimes. Kim and Hayden succeeded in modeling the behavior of materials described by small to modest dipole moments. Their model is not adequate for describing the large dipole moment materials considered here. Like the work presented in the following paragraphs, the calculations of Kim and Hayden illustrate the advantages of the Monte Carlo approach for gaining detailed information about molecular distributions.

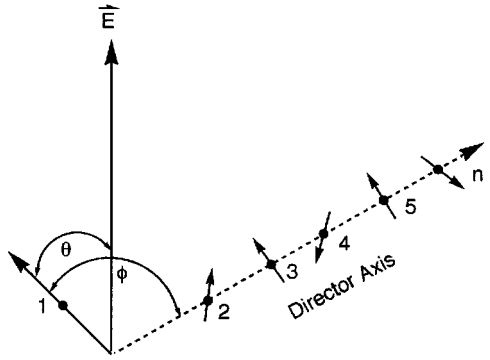

Figure 4. Shown is a series of dipoles on a one-dimensional lattice. The dipole labeled 1 is the test dipole, and the other dipoles are labeled 2 through *n*. The orientation angles for each are shown, as well as the director and external field axes.

Equilibrium Statistical Mechanical Treatment

A crucial difficulty in treating intermolecular electrostatic interactions is illustrated by Figure 4. Our problem is to compute (in a self-consistent manner) the resultant field felt by a given chromophore, which we label as 1 in Figure 4. The resultant field is the vectorial combination of fields from the applied electric field (E_p or F, corrected for medium dielectric effects) and the fields contributed by surrounding chromophores (dipolar molecules) 2 through *n*. It is clear that a very large number of orientational variables must be considered in the general formulation of this problem; not only must the rotational matrix relating chromophore 1 to the applied field be considered but also all rotational matrices relating chromophore 1 to chromophores 2 through *n* and the rotational matrices relating chromophores 2 through *n* to the applied-field (laboratory-axis) direction. The problem can be somewhat simplified, as shown in Figure 2, by placing all chromophores interacting with chromophore 1 along a "director" axis. The problem then becomes one of computing the effective field produced at chromophore 1 by chromophores 2 through *n* for each orientation of the director axis defined by the angle ϕ.

An analytical solution for relevant order parameters can be obtained by following the approach of Piekara[1] in which the mean field at chromophore 1 due to chromophores 2 to *n* is taken to be $-W\cos\phi$. In Piekara's approximation, the detailed interaction is replaced by the mean field, $-W\cos\phi$. We take W to be proportional to the average intermolecular electrostatic interaction energy, which is approximated by the pairwise particle interaction energy computed by London according to

$$W/kT = \langle E\rangle/kT = \int (E/kT)\exp(-E/kT)\,\mathrm{dE}/\int \exp(-E/kT)\,\mathrm{d}E = {}^2/_3(\mu^2/r^3kT)^2 \quad (6)$$

W/kT is on the order of the square of the norm of the nearest-neighbor interactions in the intermolecular interaction

$$|E_{DD}/kT| = \mu^2/r^3kT = N\mu^2/kT \quad (7)$$

where E_{DD} is the nearest-neighbor dipole−dipole interaction energy and r is the average separation of chromophores, assuming a uniform distribution. With this approximation, the total electrostatic interaction of eq 3 becomes $U = -\mu F\cos\theta - W\cos\phi$. The angles relating the principal axis of chromophore 1 to the poling field (θ), the principal axis of chromophore 1 to the director axis (ϕ), and the director axis, Ω, to the poling field are not independent. Making use of a well-known trigometric identity permits the number of orientational integration variables to be reduced from three to two. After some algebraic manipulation,[17] the general expression for order parameters when $f \ll 1$ can be reduced to

$$\langle\cos^n\theta\rangle = -f(\langle\langle\cos^{n+1}\theta\rangle_\theta\rangle_\Omega - \langle\cos^1\theta\rangle_\theta\langle\cos^n\theta\rangle_\Omega) \quad (8)$$

where $f = \mu F/kT$. Evaluating the integrals of eq 8, we obtain

$$\langle\cos^n\theta\rangle = -f/5\{1 - [L_1(W/kT)]^2\} \quad (9)$$

where L_1 is the first Langevin function, which is now a function of W/kT, the ratio of intermolecular electrostatic energy (W) to the thermal energy (kT). The intermolecular electrostatic interaction energy appears as an "attenuation factor", $\{1 - [L_1(W/kT)]^2\}$, that acts to oppose electric field poling-induced acentric chromophore order. The fundamental picture of the Piekara approach is an effective field from surrounding chromophores that act vectorially to oppose the applied electric poling field. Reasoning from eq 2, we find that, for $f > 1$, the acentric order parameter of eq 9 relevant to electro-optic activity becomes

$$\langle\cos^3\theta\rangle = L_3(f)\{1 - [L_1(W/kT)]^2\} \quad (10)$$

Equation 10 can be substituted into eq 1 to obtain

$$r_{33} = NL_3(f)\{1 - [L_1(W/kT)]^2\}2\beta f(\omega)/n^4 = NL_3(f)\{1 - L_1[(N\mu^2/kT)^2]^2\}2\beta f(\omega)/n^4 \quad (11)$$

From eq 11, the electro-optic coefficient, r_{33}, will depend in a much more complex way on N and μ than suggested by eq 5. A maximum is expected in the plot of r_{33} versus N, and the position of the maximum will depend on μ. We emphasize that, to obtain eq 11, we have neglected the effects of chromophore shape, i.e., nuclear repulsive interactions that act to inhibit close approach. Such interactions can be included in numerical calculations either in the "hard sphere or object" approximation or in the "soft sphere or object" approximation that includes r^{12} repulsive interactions.[17] However, such considerations of molecular shape effects generally preclude the achievement of analytical expressions.

Monte Carlo Treatment

For most of the following Monte Carlo simulations [of the effect of a poling field interacting with the second-order nonlinear optical chromophores in inert polymer matrices such as poly(methyl methacylate); PMMA; and amorphous poly(carbonate), APC], we consider only dipole−poling field and intermolecular dipole−dipole electrostatic interactions. Moreover, we initially neglect the dielectric constant of the matrix and the polarizability of the chromophores, and we assume that all chromophores are spherical in shape. With these approximations, quantitative simulation of experimental data is impossible. However, our focus here is to compare predictions of an equilibrium statistical mechanical treatment based on Piekara's approximation with those of a Monte Carlo statistical mechanical treatment. Our objective is to understand experimental observations within the framework of the simplest possible model. After we have compared equilibrium and Monte Carlo results for this simple model, we will briefly discuss the quantitative simulation of experimental results by explicitly considering shape effects.

We restrict our theoretical calculations to an investigation of the following range of variables. Chromophore dipole moments are restricted to the range $6 < \mu < 14$ D and chromophore

number densities to the range $0 < N < 20 \times 10^{20}$ molecules/cm^3. We are interested in poling fields of magnitudes in the range $100 < F < 600$ V/μm; such poling fields are obtained by corona poling and by electrode poling when conducting cladding layers are employed. For smaller poling fields, acentric(ferroelectric)/centric(antiferroelectric) second-order phase transformations are experimentally and theoretically found to be a potential problem.

With a Monte Carlo approach, the results will be numerical; an analytical solution is not possible. The approach has the advantage of permitting detailed visualization of the distribution of an ensemble of chromophores and changes in that distribution with experimental conditions. All order parameters (completely specifying the chromophore distribution) are computed with no additional computational effort. No approximations are made, but only finite systems can be considered. The results presented here are for a collection of 1000 chromophore molecules.

Our model system consists of 1000 spherical chromophore molecules (dipoles) positioned in a simple (body-centered cubic) three-dimensional ($10 \times 10 \times 10$) lattice. Each dipole resides at a lattice site, and the distance between nearest-neighbor dipoles is $N^{-1/3}$. The orientation of a dipole i is described by the angles θ_i and ϕ_i. We consider all nearest- and next-nearest-neighbor pairwise interactions and use re-entrant boundary conditions, so that the lattice is embedded in multiple copies of itself. We begin with a uniform random distribution of dipolar molecules, so that $\langle\cos^1\theta\rangle = \langle\cos^3\theta\rangle = 0$, $\langle\cos^2\theta\rangle = {}^1/_3$, and $\langle\cos^4\theta\rangle = {}^1/_5$.

The evolution of the lattice of particles is accomplished in the following manner. We choose a dipole i and move $\cos\theta_i$ and ϕ_i by $\delta(\cos\theta_i)$ and $\delta(\phi_i)$, respectively. The step sizes, $\delta(\cos\theta)$ and $\delta(\phi)$ were adjusted so that the rejection ratio for the move was $\sim{}^1/_2$. We then calculate the energy change resulting from the reorientation of the ith dipole, ΔE_i. If $\Delta E_i < 0$, we keep the move. If $\Delta E_i > 0$, we compare the value of $\exp(-\Delta E_i/kT)$, which is in the range 0−1, with a random number generated uniformly over the interval 0−1. If the move is not very large in ΔE, as the uniform random number suggests, then we keep the move. It is well-known that this procedure guarantees a Boltzmann distribution.[21]

Typically, computations begin with chromophore number densities sufficiently low that intermolecular electrostatic interactions are unimportant (see Figure 5). The set of chromophore orientations of the lattice members then evolves for a number of steps (say 200) sufficiently great to ensure that "equilibrium" has been obtained. The last 75 steps out of the 200 steps are averaged. Results are compared with the analytical theory (which, for noninteracting particles, is well-known and is shown by triangles in Figure 5). The number density is increased, and the moments, n, of $\langle\cos^n\theta\rangle$ are computed. Taking advantage of the detailed picture of the distribution provided by Monte Carlo methods, we look at various "snapshots" during the evolution process.

From a consideration of the results presented in Figure 5, it is clear that Monte Carlo calculations (steps 0−200) reproduce well the known analytical results for electric-field poling of noninteracting particles. The distribution snapshot shown in Figure 6 indicates that the most probable orientation of a chromophore dipole is collinear with but opposing the applied electric field (hence negative values for $\langle\cos^3\theta\rangle$ and $\langle\cos^1\theta\rangle$, as expected for the sign conventions of the $\mu\cdot\mathbf{E}$ interaction). When the chromophore number density increases, the magnitudes of the order parameters decrease in a manner consistent with the analytical theory of Piekara. A distribution snapshot,

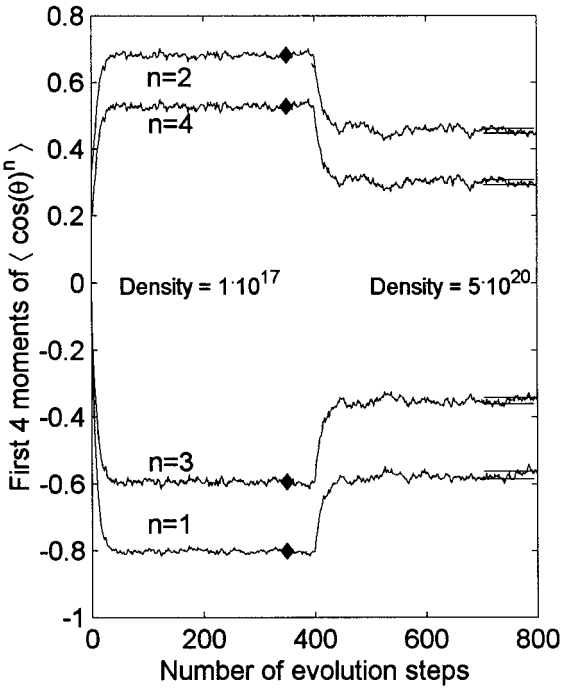

Figure 5. First four moments of the distribution of dipoles plotted as a function of the number of steps in the Monte Carlo calculation. The initial position is consistent with a random distribution. The external field is set to 600 V/μM, and each dipole moment is taken to be 13 D. The system consists of 1000 dipoles arrayed on a $10 \times 10 \times 10$ lattice. The number of steps to achieve equilibrium is around 50−70. The rejection ratio is about 0.5, as suggested elsewhere.[21] For the first 200 steps, the number density is $N = 10^{17}$ molecules/cm^3, a very low value (intermolecular interactions are unimportant). Then, the number density is increased to 10^{21} molecules/cm^3. The error bars of the calculation are the standard errors averaged over the last 75 steps. The diamonds are the analytic answers for each of the four moments, assuming no dipole−dipole interactions. The negative signs for $\langle\cos\theta\rangle$ and $\langle\cos^3\theta\rangle$ reflect the sign of the $\mu\cdot\mathbf{E}$ interaction.

shown in Figure 7, indicates that the most probable orientation of a chromophore dipole is no longer along the applied electric poling field but rather tilted with respect to the applied field. If the magnitude of the applied electric poling field is decreased or if the concentration of chromophores is increased, then the tilt angle for the most probable dipole orientation further increases (see Figure 8). The distributions shown in Figures 7 and 8 are consistent with the view that the applied electric field and the fields from surrounding dipoles add vectorially at a given chromophore to produce an effective field that defines the orientation of that chromophore in space. This is in contrast to the picture in which phase separation of centric (antiferroelectric) and acentric (ferroelectric) chromophore domains occurs. Phase separation (the detailed phase diagram) depends on the applied electric field, the chromophore number density, and the dielectric permittivity of the medium. Theory suggests that the second-order phase transition to a centric (antiferroelectric) order structure is not a problem for the high poling fields and moderate to large dipole moments considered here. We have identified conditions under which phase separation is important, but that discussion is deferred to another publication.

In Figure 9, we show graphs of $N\langle\cos^3\theta\rangle$ (which is linearly related to the electro-optic coefficient, r) versus chromophore number density, N, for different values of μ. The results of experiment and of the analytical theory of eq 11 are reproduced (certainly at least qualitatively). The role of intermolecular dipole−dipole interactions in attenuating acentric order and electro-optic activity becomes apparent: Not only is a maximum

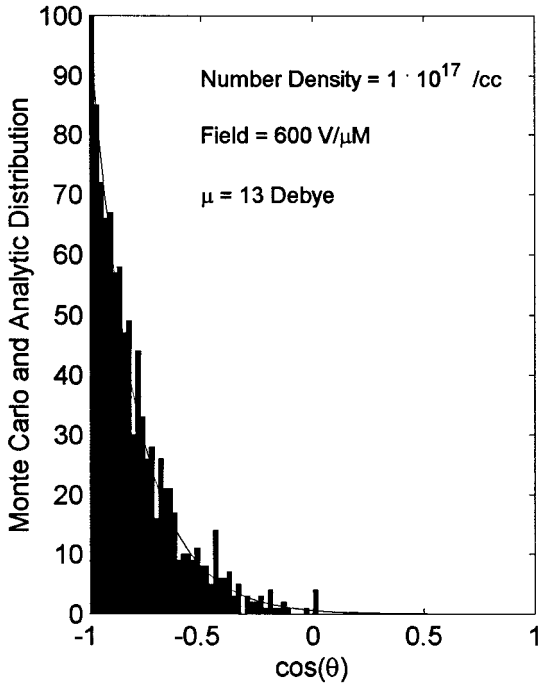

Figure 6. Histogram of the orientation of 1000 chromophores after the 400th step, plotted as a function of the cosine of the angle from the poling field. The density is $N = 10^{17}$ molecules/cm^3. Parameters are given in the Figure 6 legend. The solid line is the analytic form, assuming no dipole−dipole interactions. The histograms of Figures 6−8 are plotted on the same scales and are all normalized to 1000 counts.

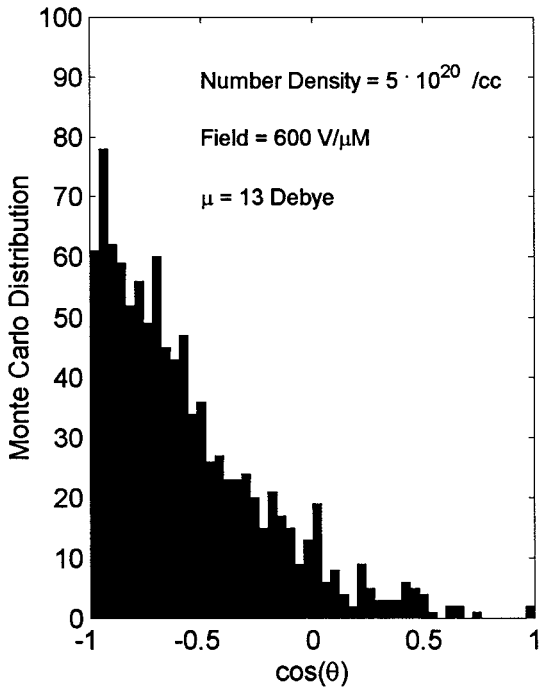

Figure 7. Histogram of the orientation of the 1000 chromophores after 400 steps of evolution from the configuration of the previous figure, plotted as a function of the cosine of the angle from the poling field. The density is $N = 5 \times 10^{20}$ molecules/cm^3. The histograms of Figures 6−8 are plotted on the same scales and are all normalized to 1000 counts.

predicted in the plots $N\langle\cos^3\theta\rangle$ versus N but the position of the maximum shifts to lower N with increasing μ (in agreement with experiment and with analytical theory). The standard error of the calculation is shown with each datum; the larger-scale oscillations in the calculations indicate a response to being

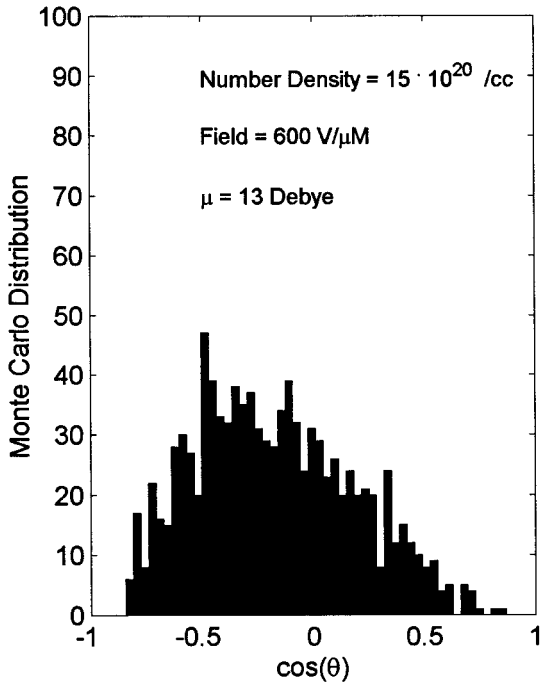

Figure 8. Histogram of the orientation of 1000 chromophores after the 400th step from the configuration shown in the previous figure, plotted as a function of the cosine of the angle from the poling field. The density is $N = 15 \times 10^{20}$ molecules/cm^3. The histograms of Figures 6−8 are plotted on the same scales and are all normalized to 1000 counts.

kinetically trapped in local minima. This was demonstrated by noting that the results were dependent on the step size of the chromophore density and the direction of density change. In Figure 10, we illustrate a more detailed comparison of the predicted functional dependence of $N\langle\cos^3\theta\rangle$ on N for Monte Carlo and analytical theories. The two different loading curves (which were computed for two different poling field strengths that differ by a factor of 2) show how each of the theories scales with poling field. Clearly, there is reasonable agreement in the functional dependence predicted by the quite different theoretical methods. We believe that, among other points, the comparison shown in Figure 10 provides important support for the physical reasonableness of the approximation advanced by Piekara.

Figure 11 compares the Monte Carlo generated loading curves for two different lattice geometries. The curve that extends to higher loading values is that for a uniform lattice. The lower two curves are two separate calculations of the loading curve for a lattice in which the spacing of lattice points in the direction of the poling field is three times that of the spacing of the lattice points in the other two directions. This distorted (tetragonal) lattice is intended to simulate the effect of considering prolate ellipsoids with a 3:1 aspect ratio. However, at high loading, no evidence in the histograms was seen of centrosymmetric (antiferroelectric) ordering. The predominant orientations of the chromophores were perpendicular to the poling field. Hence, even under extreme conditions that could promote the formation of centrosymmetric aggregates, no such aggregates were formed.

In Figure 12, we explicitly take chromophore shape and nuclear repulsive interactions into account by treating the chromophores as hard-shell ellipsoids with the ellipsoidal shape determined from quantum mechanical calculations. The calculations were carried out under the restriction that no two chromophores could occupy the same space at the same time. At low chromophore concentrations, shape effects are unimportant. Chromophore distributions are homogeneous and can

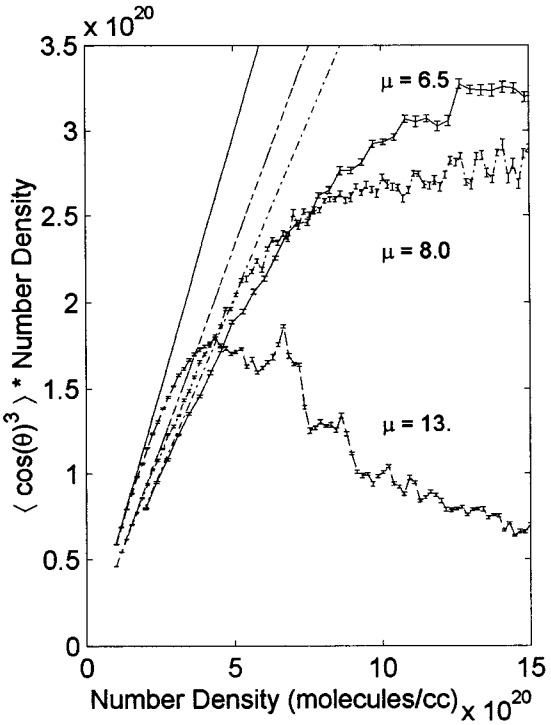

Figure 9. Graph of $\{N\langle\cos^3\theta\rangle\}$ (which is linearly related to r_{33}) as a function of N, chromophore number density, for the following different values of μ: $\mu = 6$ (solid line), 8 (dash−dot), and 13 (dash) D. The error bars are the standard errors of each value, obtained by averaging 75 steps in the Monte Carlo simulations. The dashed straight lines are the analytic theory, assuming no dipole−dipole interactions (see eq 4). We chose to plot $\{N\langle\cos^3\theta\rangle\}$, rather than r_{33}, because the dependence of the latter on the molecular first hyperpolarizability, β, and the host dielectric constant, ϵ, obscures the trends that we wish to emphasize. That is, $\{N\langle\cos^3\theta\rangle\}$ more directly illustrates the attenuating role of intermolecular electrostatic interactions.

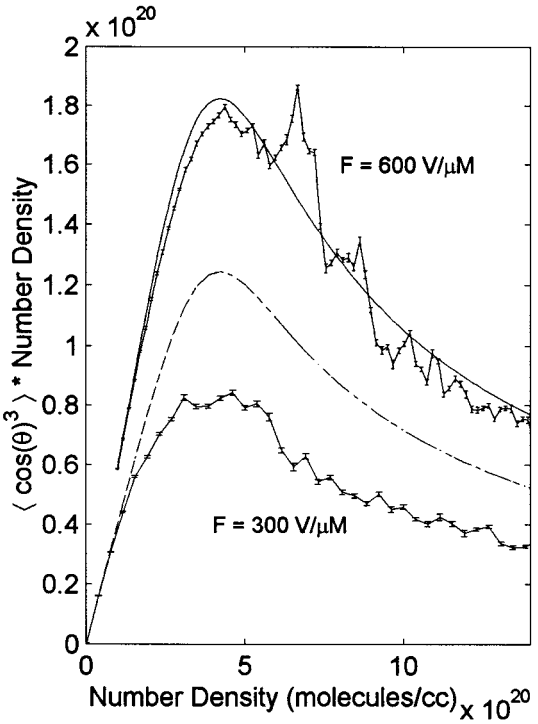

Figure 10. Graph of $\{N\langle\cos^3\theta\rangle\}$ as a function of N, chromophore number density, for $\mu = 13$ D and external poling fields of 300 and 600 V/μM. The straight, dashed lines show results from eq 4. The two solid lines use the analytic theory of Piekara for the third moment of the distribution (see eq 10).

be described as a cubic lattice. As chromophore average intermolecular distances approach chromophore long-axis lengths, a transition to a tetragonal lattice occurs. Chromophore rotational motion becomes restricted in the high-concentration regime. In addition to showing the simulation (solid line) of experimental data (diamonds) for the CLD-OMet chromophore in PMMA, we also show in Figure 12 the deconvolution of the total theoretical curve into electronic and nuclear repulsive (shape) effects. The electronic effect (short dashes) is what would be observed if the chromophores were spherical. The nuclear repulsive contribution (long dashes) sets in at higher concentrations than does the electronic electrostatic effect but clearly is important at high concentrations.

The agreement between theory and experiment shown in Figure 12 is good but less than exact. Note that the theoretical results shown in this figure were computed without using adjustable parameters and without considering higher-order effects, as discussed. When higher-order interactions are considered in a self-consistent manner, excellent agreement between theory and experiment is obtained (see Figure 2 for an example of the level of agreement that is obtained). An important observation to be derived from Figure 12 is that such higher-order treatment is not necessary to understand experimental trends or to design improved chromophores. Part of the reason for the good agreement of the more approximate theory with experiment is serendipitous because of the partial cancellation of higher-order contributions of different signs. For example, the host dielectric constant influences both the poling field felt by a given chromophore and the field from surrounding chromophores felt by that chromophore, but the effects have opposite influences on the value of $\langle\cos^3\theta\rangle$.

Conclusions

The calculations presented in this article establish a consistency between the Monte Carlo method and analytical theory based on Piekara's approximation. This consistency is quite important, as these two calculation methods represent quite different theoretical approaches to the same problem. An important result is that even this simple picture of interacting chromophores (in which the polarizability, shape of the chromophore, and the dielectric nature of the medium are neglected) qualitatively reproduces most of the essential features of experiment. The essential features are the following: (1) A maximum value is found in the graph of the electro-optic coefficient (r_{33}) as a function of chromophore number density (N). (2) The maxima in graphs of r_{33} versus N shift to lower values of N with increasing chromophore dipole moment (μ). (3) The detailed shape of the functional form of the dependence of r_{33} on N is qualitatively reproduced by the calculations.

The Monte Carlo method has the advantage, relative to equilibrium statistical mechanical methods, of providing detailed insight into the distribution of molecules (dipoles). It is thus more physically intuitive. A subtle, but important, observation of the calculations presented here is that phase separation into acentric and centric domains (aggregates) is not observed for the model systems considered. The competition of the poling field and intermolecular electrostatic interactions can, thus, be viewed from the standpoint of an "effective field" picture in which the most probable chromophore orientation is defined by the vectorial resultant of the poling field with fields contributed by surrounding dipolar molecules. This result is consistent with a variety of experimental observations, including the detailed functional dependence of r on N, the absence of

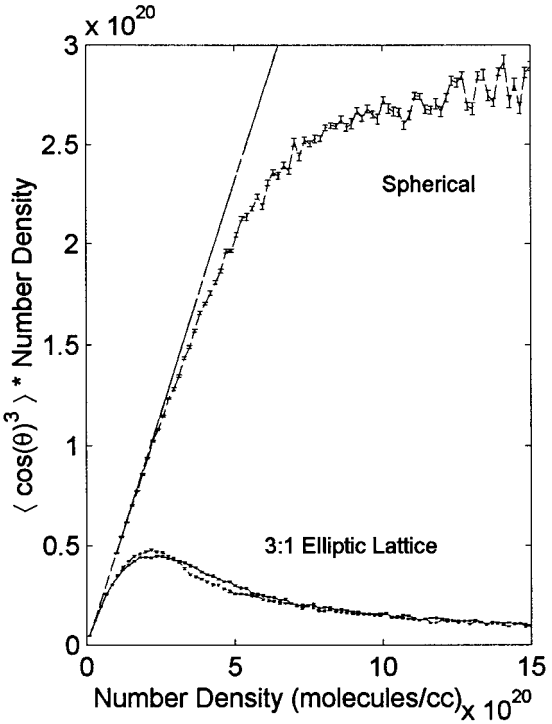

Figure 11. Plot of $\{N\langle\cos^3\theta\rangle\}$ as a function of N, chromophore number density, for $\mu = 8$ D and for two different lattice geometries. The plot labeled Spherical uses a uniform lattice. The two plots labeled 3:1 Elliptic Lattice use a lattice in which the distance between dipoles is three times larger in the poling field direction than in the other two directions. The two plots are two separate calculations, which differ in the number of nearest neighbors included in the interaction energy of each chromophore. In one calculation, 26 nearest neighbors were included, and in the other calculation, 125 nearest neighbors were included. The results are essentially identical.

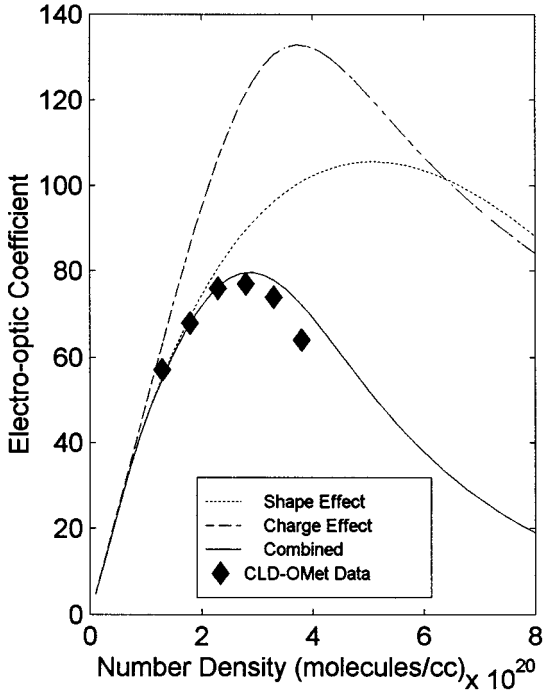

Figure 12. Experimentally observed (diamonds) and theoretically predicted (solid line) variation of electro-optic coefficient versus chromophore number density for the CLD-OMet chromophore in PMMA. CLD-OMet involves replacement of the H with the methoxy group. The theoretical curve was computed as discussed in the text with the restriction that chromophores are treated as hard-shell (non-interpenetrating) ellipsoids. At high concentrations, some rotational motions for a given chromophore become restricted by the requirement that two chromophores cannot occupy the same space at the same time. This figure also shows the deconvoluted functional dependence of the electrostatic effect (purely electronic, denoted charge effect, short dashes) and nuclear repulsive effect (denoted shape effect, long dashes). The purely electronic effect is what would be observed for a spherical chromophore. Note that the scale to the right of the figure applies only to the experimental data and theoretical curve (solid line) corresponding to the total contributions of electronic and shape effects. As expected and as is evident from this figure, the electronic effect is longer range and sets in at a lower chromophore concentration than the shape effect, but the shape effect makes an important contribution at higher concentrations.

light scattering from aggregates, the relationship between electro-optic activity and birefringence, and the results of pulsed poling field experiments. Even more encouraging, the present results help to identify the small number of systems in which phase separation into centric and acentric (noncentrosymmetric) phases has been observed. The Monte Carlo method provides an attractive formalism for theoretically exploring such effects.

The simple model and Monte Carlo calculations presented here can be executed on most personal computers. The Monte Carlo method is a facile way of qualitatively (and even semiquantitatively) exploring the dependence of the electro-optic coefficient for a new chromophore material on chromophore number density, applied electric field, and the dipole moment of the chromophore. With greater computational capability, the method is readily adapted to incorporate considerations of chromophore shape, the dielectric nature of the medium, the details of the sample and poling configuration, etc. These activities, which rely on Piekara's fundamental approximation of interacting dipolar molecules,[17] have already been executed within the framework of numerical equilibrium statistical mechanics. Monte Carlo calculations not only provide support for such calculations but also provide a more intuitive approach for treating higher-order effects.

Relation of Theory to Future Experiments. The theoretical and experimental results unequivocally refute the concept that $\mu\beta$/MW is a useful scaling parameter for predicting the utility of newly prepared second-order nonlinear optical chromophores. Expectations for ultrafast "purely electronic" electro-optic activity must be correspondingly lowered. With existing chromophores, it is unrealistic to think of constructing neat chromophore lattices that exhibit electro-optic activity that will compete with liquid crystalline materials in beam-steering applications. There is simply no way to avoid experiencing some reduction in macroscopic electro-optic activity associated with intermolecular electrostatic (electronic and nuclear) interactions. Theory fortunately tells us how to minimize such attenuation of electro-optic activity. One approach to minimizing the attenuation is to control chromophore shape. While a detailed discussion of this topic is outside the realm of the present discussion, we note that there are a number of approximate methods for considering chromophore shape (e.g., see Figures 2, 11, and 12).[17] Each of these methods supports the fundamental conclusion that prolate ellipsoidal chromophore shapes are undesirable. Electro-optic activity is theoretically predicted and experimentally observed to be considerably improved (e.g., by factors of 2 or more) by adding inert (sterically bulky) substituents to inhibit close side-by-side (along the minor axes of the prolate ellipsoids) approach of chromophores. A synthetic scheme well suited to such chromophore modification is that of dendrimer synthesis, but even simple derivatization with alkyl and alicyclic substituents can be effectively employed.[3] The ideal chromophore shape is that of a sphere. Theory can provide useful guidance for the most appropriate modification of a given

π-electron backbone structure. Such derivatization can also be used to control solubility and processability, to improve chemical and photochemical stability, to facilitate lattice-hardening schemes carried out after electric-field poling, and to minimize optical loss due to vibrational absorption by exploiting selective halogenation and isotopic substitution.

Theory can also provide more subtle guidance. For example, cases in which pulsed poling techniques can be effectively utilized can be identified, the role of the host dielectric constant can be clarified, etc. Note that the role of the polymer host dielectric constant (dielectric permittivity) is more complex in the presence of large intermolecular electrostatic interactions. In the absence of such interactions, the dielectric nature of the host polymer acts only to attenuate the magnitude of the applied electric poling field felt by the dipolar chromophores of the sample. The prediction of independent particle theory is that the lower the dielectric constant of the medium, the better. Indeed, the very high dielectric constant of crystalline lithium niobate ($\epsilon = 28-80$, depending on crystal orientation) is a distinct disadvantage.[22] However, a modest dielectric constant for a polymer host is an advantage for chromophores experiencing large intermolecular electrostatic interactions, as the dielectric nature of the medium acts to attenuate these interactions. For example, dissolving the CLD chromophore into amorphous poly(carbonate), APC [polybisphenol A carbonate-*co*-4,4′-(3,3,5-trimethylcyclohexylidene)diphenol], rather than PMMA increases the maximum observed electro-optic coefficient by approximately 10 pm/V. Of course, all theories predict that the higher the poling field strength, the better. Unfortunately, dielectric breakdown limits the magnitude of the applied electric fields that can be employed in electric-field poling. We should also indicate that the phase transition from a "homogeneous or effective field" chromophore lattice to phase-separated centric/acentric domains depends on N, F, and ϵ. The high electric fields produced by corona poling or by electrode poling with conducting cladding layers[23] oppose phase separation, but even for such experiments, phase separation is observed for a small number of materials and conditions.

We emphasize that the theory developed here is also relevant to the understanding of electro-optic materials fabricated by self-assembly methods such as the Langmuir−Blodgett film fabrication method. For such assembly, the orientation of chromophores with respect to the substrate surface is influenced by intermolecular electrostatic interactions. Chromophores tilt away from the normal to the substrate surface under the influence of intermolecular electrostatic interactions. This tilting reduces the electro-optic activity. The same observations concerning chromophore shape and number density apply to this situation as to electric-field poling. The only difference is that surface forces replace the poling field in driving acentric order. Because anchoring forces of sequential synthesis methods can be very large (e.g., because of covalent bond formation), this is an argument for the ultimate potential advantage of these techniques over poling methods.

Theoretical calculations have already helped guide the development of polymeric electro-optic materials characterized by electro-optic coefficients of greater than 100 pm/V, yielding devices with drive voltage requirements of ≤ 1 V.[12,13] With continued minor modifications of existing chromophore structures, it is now clear that device drive voltages can be reduced to less than 0.5 V. Indeed, chromophores with extended polyene bridges protected by two or three fused alicyclic ring systems have been prepared, yielding electro-optic coefficients greater than 100 pm/V.[3] The two-ring version, referred to as GLD, is already being used in the fabrication of prototype devices with improved electro-optic activity. Exceptional electro-optic activity (>100 pm/V) and excellent thermal stability have also been obtained by the inclusion of dithiophene units into protected polyene bridge structures.[3,14] Replacement of the furan oxygen of CLD with a variety of functionalities has led to improved chromophores, and promising results are being obtained for a variety of dendrimer materials based on CLD, GLD, and related chromophores.[3] With expected continued improvement in chromophore hyperpolarizability and with theoretically guided design of optimum chromophore shapes, it is reasonable that drive voltages of 0.1−0.4 V will be achieved in the not too distant future. With the limitations imposed by intermolecular electrostatic interactions, drive voltages of 0.01 V will be extremely difficult, if not impossible, to achieve. Thus, the future of polymeric electro-optic materials is extremely bright for satellite- and optical fiber-based telecommunications, phased-array radar, electronic counter measures (ECM), land mine detection, optical gyroscopes (guidance systems), information processing (ultrafast analog-to-digital conversion), switching at nodes in local area optical networks, and remote high-voltage sensing (transformer voltage fluctuations). However, direct sensing of weak electromagnetic fields (e.g., semiconductor diode replacement for broad bandwidth magnetic resonance) and large-angle beam-steering applications appear unlikely. It is conceivable that spatial light modulation will be achieved by making use of new polymeric electro-optic materials incorporated into photonic band-gap structures.

As noted in the Introduction, the theory developed here is also relevant to a number of other technologically significant observations, including those involving photorefractive, liquid crystalline, and organic light-emitting diode materials.

Acknowledgment. We gratefully acknowledge the support of this work by the National Science Foundation and by the U.S. Air Force Office of Scientific Research.

References and Notes

(1) London, F. *Trans. Faraday Soc.* **1937**, *33*, 8. London, F. *Z. Phys. Chem., Abt. B* **1930**, *11*, 222. London, F. *Z. Phys.* **1930**, *63*, 245. Piekara, A. *Z. Phys.* **1938**, *108*, 395. Piekara, A. *Proc. R. Soc. London, A* **1939**, *172*, 360. Debye, P. *Phys. Z.* **1935**, *36*, 100. Onsager, L. *J. Am. Chem. Soc.* **1936**, *58*, 1486. Fowler, R. H. *Proc. R. Soc. London, A* **1935**, *149*, 1. Ehrenson, S. J. *Comput. Chem.* **1989**, *10*, 77. Israelachvili, J. N. *Intermolecular and Surface Forces*; Academic Press: London, 1985. Hansen, J. P.; McDonald, I. R. *Theory of Simple Liquids*; Academic Press: London, 1976. Chandler, D. *Introduction to Modern Statistical Mechanics*; Oxford University Press: Oxford, 1987. Uzunov, D. I. *Introduction to the Theory of Critical Phenomena: Mean Fields, Fluctuations, and Renormalization*; World Scientific: Singapore, 1993. Ma, S. K. *Modern Theory of Critical Phenomena*; W. A. Benjamin: Reading, MA, 1976. Smart, J. S. *Effective Field Theories of Magnetism*; Saunders: Philadelphia, PA, 1966.

(2) Boulbitch, A.; Toledano, P. *Phys. Lett.* **1999**, *A237*, 271. Lalanne, P. J.; Marcerou, J. P. *Phys. Rev. E* **1995**, *52*, 1846. Toledano, P.; Amf, N.; Aa, B.; *Phys. Rev. E* **1999**, *59*, 6785. Mottram, N. J.; Elston, S. J. *Liq. Cryst.* **1999**, *26*, 457.

(3) Dalton, L. R.; Steier, W. H.; Robinson, B. H.; Zhang, C.; Ren, A. S.; Garner, S. M; Chen, A.; Londergan, T.; Irwin, L.; Carlson, B.; Fifield, L.; Phelan, G.; Kincaid, C.; Amend, J.; Jen, A. K. Y. *J. Chem. Mater.* **1999**, *9*, 1905. Dalton, L. R.; Harper, A. W.; Ren, A. S.; Wang, F.; Todorova, G.; Chen, J.; Zhang, C.; Lee, M. *Ind. Eng. Chem. Res.* **1999**, *38*, 8. Dalton, L. R. Polymers for Electro-Optic Modulator Waveguides. In *Electrical and Optical Polymer Systems: Fundamentals, Methods, and Applications*; Wise, D. L., Cooper, T. M., Gresser, J. D., Trantolo, D. J., Wnek, G. E., Eds.; World Scientific: Singapore, 1998; p 609. Dalton, L. R. Nonlinear Optical Polymeric Materials: From Chromophore Design to Commercial Applications. In *Advances in Polymer Science*; Springer-Verlag: Heidelberg, Germany, 2000, in press. Nalwa, H. S.; Miyata, S. *Nonlinear Optics of Organic Molecules and Polymers*; CRC Press: Boca Raton, FL, 1997. Dalton, L. R.; Harper, A. W. *Polym. News* **1998**, *23*, 114.

(4) Chen, D.; Fetterman, H. R.; Chen, A.; Steier, W. H.; Dalton, L. R.; Wang, W.; Shi, Y. *Proc. SPIE* **1997**, *3006*, 314. Chen, D.; Fetterman,

H. R.; Chen, A.; Steier, W. H.; Dalton, L. R.; Wang, W.; Shi, Y. *Appl. Phys. Lett*. **1997**, *70*, 3335. Chen, D.; Bhattacharya, D.; Udupa, A.; Tsap, B.; Fetterman, H. R.; Chen, A.; Lee, S. S.; Chen, J.; Steier, W. H.; Dalton, L. R. *IEEE Photonics Technol. Lett.* **1999**, *11*, 54.

(5) Chen, A.; Chuyanov, V.; Marti-Carrera, F. I.; Garner, S. M.; Steier, W. H.; Chen, J.; Sun, S.; Dalton, L. R. *Proc. SPIE* **1997**, *3005*, 65. Garner, S. M.; Lee, S. S.; Chuyanov, V.; Yacoubian, A.; Chen, A.; Steier, W. H.; Zhu, J.; Chen, J.; Wang, F.; Ren, A. S.; Dalton, L. R. *Proc. SPIE* **1998**, *3491*, 421. Garner, S. M.; Lee, S. S.; Chuyanov, V.; Chen, A.; Yacoubian, A.; Steier, W. H.; Dalton, L. R. *IEEE J. Sel. Top. Quantum Electron*. **1999**, *35*, 1146. Steier, W. H.; Chen, A.; Lee, S. S.; Garner, S. M.; Zhang, H.; Chuyanov, V.; Dalton, L. R.; Wang, F.; Ren, A. S.; Zhang, C.; Todorova, G.; Harper, A. W.; Fetterman, H. R.; Chen, D.; Udupa, A.; Bhattacharya, D.; Tsap, B. *Chem. Phys*. **1999**, *245*, 487.

(6) Lee, S. S.; Udupa, A. H.; Erlig, H.; Zhang, H.; Chang, Y.; Zhang, C.; Chang, D. H.; Bhattacharya, D.; Tsap, B.; Steier, W. H.; Dalton, L. R.; Fetterman, H. R. *IEEE Microwave Guided Wave Lett.* **1999**, *9*, 357.

(7) Chen, R.; Li, B.; Chen, Y.; Fu, Z.; Steier, W. H.; Dalton, L. R.; Fetterman, H. R.; Lee, C. *Proc. PSAA* **2000**, in press. Steier, W. H.; Oh, M. C.; Zhang, H.; Szep, A.; Dalton, L. R.; Zhang, C.; Fetterman, H. R.; Chang, D. H.; Erlig, H.; Tsap, B.; Shi, Y.; Bechtel, J. H.; Lin, W.; Chen, R.; Lee, C. Y. C. *Proc. PSAA* **2000**, in press. Fetterman, H. R.; Chang, Y.; Erlig, H.; Tsap, B.; Oh, M. C.; Zhang, C.; Steier, W. H.; Dalton, L. R.; Chen, R.; Lee, C. *Proc. PSAA* **2000**, in press.

(8) Chang, D. H.; Erlig, H.; Fetterman, H. R.; Oh, M. C.; Steier, W. H.; Dalton, L. R. *IEEE Photonics Technol. Lett*. **2000**, in press.

(9) Dalton, L. R.; Steier, W. H.; Robinson, B. H.; Zhang, C.; Ren, A. S.; Garner, S. M.; Chen, A.; Londergan, T.; Irwin, L.; Carlson, B.; Fifield, L.; Phelan, G.; Kincaid, C.; Amend, J.; Jen, A. K. Y. *J. Chem. Mater.* **1999**, *9*, 1905 (see Figures 7 and 8).

(10) Shi, Y.; Wang, W.; Bechtel, J. H.; Chen, A.; Garner, S. M.; Kalluri, S.; Steier, W. H.; Chen, D.; Fetterman, H. R.; Dalton, L. R.; Yu, L. P. *IEEE J. Quantum Electron*. **1996**, *2*, 289. Shi, Y. Lucent Technologies. Private communication. Grote, J. G. AFRL/MLPO, Dayton, OH. Private communication. Ermer, S. Lockheed-Martin, Palo Alto, CA. Private communication.

(11) Kanis, D. R.; Ratner, M. A.; Marks, T. J. *Chem. Rev.* **1994**, *94*, 195. Marder, S. R.; Gorman, C. B.; Meyers, F.; Perry, J. W.; Bourhill, G.; Bredas, J. L.; Pierce, B. M. *Science* **1994**, *265*, 632.

(12) Shi, Y.; Lin, W.; Olson, D. J.; Bechtel, J. H.; Zhang, H.; Steier, W. H.; Zhang, C.; Dalton, L. R. *Science* **2000**, *288*, 119. Dalton, L. R. *OSA Technol. Dig. Org. Thin Films Photonics Appl.* **1999**, 16. Shi, Y.; Lin, W.; Olson, D. J.; Bechtel, J. H.; Wang, W. *OSA Technol. Dig. Org. Thin Films Photonics Appl.* **1999**, 20.

(13) Ermer, S.; Girton, D. C.; Dries, L. S.; Taylor, R. E.; Eades, W.; Van Eck, T. E.; Moss, A. S.; Anderson, W. W. *Proc. SPIE* **2000**, *3949*, in press.

(14) Liakatas, I.; Cai, C.; Bosch, M.; Jager, M.; Bosshard, Ch.; Gunter, P.; Zhang, C.; Dalton, L. R. *Appl. Phys. Lett*. **2000**, *76*, 1368.

(15) Harper, A. W.; Sun, S.; Dalton, L. R.; Garner, S. M.; Chen, A.; Kalluri, S.; Steier, W. H.; Robinson, B. H. *J. Opt. Soc. Am. B* **1998**, *15*, 329.

(16) The four fields typically considered include the applied poling field, the dipole−dipole field, the Lorentz field, and the depolarization field.

(17) Dalton, L. R.; Harper, A. W.; Robinson, B. H. *Proc. Natl. Acad. Sci. U.S.A.* **1997**, *94*, 4842. Robinson, B. H.; Dalton, L. R.; Harper, A. W.; Ren, A. S.; Wang, F.; Zhang, C.; Todorova, G.; Lee, M.; Aniszfeld, R.; Garner, S. M.; Chen, A.; Steier, W. H.; Houbrecht, S.; Persoons, A.; Ledoux, I.; Zyss, J.; Jen, A. K. Y. *Chem. Phys*. **1999**, *245*, 35.

(18) Katz, H. E.; Schilling, M. L., Cahill, P. A. *J. Opt. Soc. Am. B* **1990**, *7*, 309.

(19) Yitzchaik, S.; Di Bella, S.; Lundquist, P. M.; Wong, G. K.; Marks, T. J. *J. Am. Chem. Soc*. **1997**, *119*, 3091. Di Bella, S.; Lanza, G.; Fragala, I.; Yitzchaik, S.; Ratner, M. A.; Marks, T. J. *J. Am. Chem. Soc*. **1997**, *119*, 3099. Lundquist, P. M.; Yitchaik, S.; Marks, T. J.; Wong, G. K.; Di Bella, S.; Cohen, R.; Berkovic, G. *Phys. Rev. B: Condens. Matter Mater. Phys.* **1997**, *55*, 14055.

(20) Kim, W. K.; Hayden, L. M. *J. Chem. Phys*. **1999**, *111*, 5212.

(21) Allen, M. P.; Tildesley, D. J. *Computer Simulation of Liquids*; Clarendon Press: Oxford, 1987; Chapter 4.

(22) Dalton, L. R.; Harper, A. W.; Ghosn, R.; Steier, W. H.; Ziari, M.; Fetterman, H. R.; Shi, Y.; Mustacich, R. V.; Jen, A. K. Y.; Shea, K. *J. Chem. Mater*. **1995**, *7*, 1060.

(23) J. G. Grote, U.S. Air Force Research Laboratory (AFRL/MLPO), Wright-Patterson Air Force Base, Dayon, OH. Private communication. Use of conducting cladding layers effectively reduces the electrode gap to that of the active poling layer while providing isolation of the active material from the metal electrodes. Such (cladding layer) isolation of the active electro-optic layer from metal electrodes is important for avoiding high optical loss from propagating light seeing the active device electrode (which may or may not be the poling electrode) and from material damage of the active electro-optic layer due to high fields associated with needlelike areas existing over the electrode surface. Use of conducting cladding layers permits an increase of the effective poling field felt by the chromophores of the active layer. For the CLD/PMMA composite material of Figure 1, use of an active cladding layer improves the maximum achievable electro-optic coefficient by approximately 10−15 pm/V.